Jet Measurements with High-Vision 3D-PTV

D. H. Doh*, D. H. Kim*, Y. B. Cho*, T. Saga**, T. Kobayashi**, Y. B. Pyun***

* *Division of Mech. & Info. Eng., Korea Maritime Univ., doh@hanara.kmaritime.ac.kr*
** *Institute of Industrial Science, Tokyo University, kobaya@iis.u-tokyo.ac.jp*
***TNTech Co., flowtech@tientech.com*

Abstract   A new GA-3D-PTV technique has been constructed to measure an impinging jet. The measurement system consists of three CCD cameras, Ar-ion laser, an image grabber and a host computer. GA (Genetic Algorithm) was used based on one-to-one correspondences in order to take advantage of the combinatorial optimization in tracking the pairs of the whole particles of the two images having a time interval. Two fitness functions were introduced in order to enhance the correspondences of the particles. One was based on a concept of the continuum theory and the other one was based on a minimum distance error. The constructed GA-3D-PTV system was applied in success to the measurement of flow characteristics of the impinging jet.

1. Introduction

Impinging jets are characterized by unusually high transfer coefficients near the stagnation region. For this reason, they are found in wide application in a variety of industries such as, cooling turbine-blade and the surface of combustor and a semiconductor in the electronic equipment. Impinging jet can be adopted many times for its outstanding cooling efficient of high-temperature plate. Submerged impinging jets have received substantially more attention in the literature than have impinging free liquid jets. There has been interest in using impinging jets to dissipate the high heat fluxes found in electronic equipment such as VLSI circuits (Kiper, 1984; Yamamoto et al., 1987).

The stagnation point velocity gradient had been shown by many pervious analytical and experimental investigations to be an important parameter in stagnation heat transfer (Sibulkin, 1952; Burmeister, 1983 Vader et al., 1991). The magnitude of the heat transfer coefficient found to be influenced by the stagnation line velocity gradient so that a narrower jet provided higher heat transfer coefficients. Several related factors, including the jet exit velocity profile, and stagnation region radial velocity gradient have been proposed to be of importance in governing the heat transfer under an impinging jet (Stevens and Webb, 1991; Vader et al., 1991). All of these factors are known to influence the heat transfer on the surface of the impinging plate.

Olsson and Turkdongan (1966) investigated experimentally the radial flow field of an impinging liquid jet with pointwise measurement results. Nakoryakov et al. (1978) discussed the flow field of an impinging jet in an experimental and theoretical study on the mass transfer and friction factor under such a jet. Gardon et al. (1965) discovered how the turbulent flow can effect heat transfer when free jet was impinged on the surface of a plate. Kataoka et al. (1986) discovered through pointwise measurements that period of vortex could change the effect of heat transfer at the impinging plate after observating a large period vortex on the round nozzle jet. Stevens et al. (1991, 1992) investigated the effect of nozzle configuration with the results of LDV experiments.

Most of the results obtained by previous researches were based on a pointwise measurement technique such as, Hot wire and LDV, or numerical simulations. No matter how the numerical results are accurate, the results should be proved with the results obtained through an experiment because the flow fields are too complicate to be analyzed accuratly. In order to attain accurate analysis on the impinging jet, it is necessary to know vortical structures of the jet. There have been some efforts to study the influence of the flow structures of an impinging jet on heat transfer.

Faggiani and Grassi (1990a, 1990b) studied the influences of the local and average heat transfer characteristics by studying the influence of flow structure on transport as their main

focuses. However, they showed their results on large-scaled flow structures. Hwang (1999) investigated the influences of the arrangement of an impinging jet. Lee et al. (1999) investigated heat transfer characteristics at the nozzle exit configuration of turbulence axisymmetric impinging jet. Kim et al. (2001) investigated the influence of the impinging angles with PIV. They could get their results with a fieldwise measurement, PIV (Particle Image Velocimetry) and LCM(Liquid Crystal Method). However, the results proposed by them were based on 2-dimensional PIV technique or 2-dimensional-field measurement technique. To make a complete analysis on the influences of the flow structures of the jet, it is even more necessary to investigate the flows 3-dimensionally as the structures have strong 3-dimensionality. None of the previous studies reports on the influences of the flow structures with the results that contain 3-dimensional properties in space except some studies reported through numerical simulations. This means that a measurement technique that can measure an instantaneous vortical structures of the jet with high resolutions is necessary in order to attain more accurate study into the influences of the vortical structures of the impinging jet on the heat transfer of heated plates.

This study focues on an investigation into flow properties of an impinging jet with a 3D-PTV (3-Dimensional Particle Tracking Velocimetry). In Particle Tracking Velocimetry (PTV)(Adrian, 1991), increasing the number of instantaneous 3-dimensional vectors has been a hot issue. Kasagi and Nishino (1989) were able to get about 400 instantaneous three-dimensional velocity vectors for a two-dimensional channel flow by using three CCD cameras. Mass et al. (1993) could get more than 1000 instantaneous three-dimensional velocity vectors for three-dimensional channel flow with a three-camera arrangement. Doh et al. (2000) could get about 500 instantaneous three-dimensional velocity vectors for a relatively complex flow field, the flow field near the wake of a backward-facing step, by applying a match probability concept (Ballard and Brown, 1982) in pairing the particles of the two different images. They measured turbulent properties such as turbulent intensities, Reynolds stress and etc. In order to get the information of instantaneous flow structures, more than 700 instantaneous three-dimensional velocity vectors are required in a simple flow (Kasagi and Nishino, 1991).

In the mean while, Yamada (1995) and Ohyama et al. (1993) adopted the genetic algorithm (Goldberg, 1985) to PTV in order to increase the number of obtained vectors. They defined a fitness function in which the displacements of every particle's pair were assumed to be minimum value. They applied their GA-PTV algorithms to the measurement of a forced vortex flow field and obtained about 80% of correct vectors from initial velocity vectors. Doh et al. (2001) gained more than 98% of correct vectors from initial velocity vectors for the same flow field with virtual images. They took a consideration into the disappearing particles' pairs between two image frames. Their idea was to preserve a recessive group of the particles that were generally thrown away in the calculation process of genetic algorithm. Most of the conventional PTVs or GA-PTVs were mainly concerned with two-dimensional measurements.

In this study, a new High-Vision 3D-PTV system was constructed by adopting a new GA-PTV algorithm for the study of an impinging jet. The measurement system could obtain more than 5,000 instantaneous three-dimensional velocity vectors for an impinging jet with two High-Vision cameras (1016 x 1000 pixels). Several results have successfully been obtained by the constructed system. It was verified that the constructed 3D-PTV system will be able to be compatible with the results of DNS if proper resolusive cameras are systematically installed with some measures.

2. High-Vision 3D-PTV system
In order to construct a High-Vision 3D-PTV system, high-resolution cameras (Kodak ES1.0, 1,016 x 1,000 pixels) and an image grabber were constructed with 3D-PTV algorithm. To get the three-dimensional velocity vectors, exterior parameters of camera such as, the position and the orientations of the camera, interior parameters representing the focal length, deviations of the principal point and the distortion coefficients of the camera lens was obtained in advance. Next, three-dimensional position of each particle was calculated. Finally, three-dimensional velocity vectors were calculated. The second step is called as a camera calibration process.

7

2.1 Definition of camera parameters and calculations of 3D positions of particles

To make the camera calibration, the landmarks of which 3-dimensional positions are known should be used. Fig. 1 shows how the calibration for cameras was made. Three cameras were calibrated for the landmarks as shown on this figure. A traverse had been moved in stepwise to each position at which picturing by the cameras had been made. On the tip of the traverse, a ball (diameter: 2mm, accuracy: 20μm) was installed. This ball was moved three-dimensionally with 6mm interval between the positions. The images of the particles at every position were captured by the three cameras. The traversing region was 30 x 30 x 30mm. The calibration was made using these landmarks and their photographic coordinates of the three cameras. Some processing such as noise reduction and thresholding were carried out on the images to get more accurate photographic coordinates of landmarks.

Nishino (1989) and Doh et al. (2000) used 11 parameters that crucially decide the camera's orientation. However, the whole processes obtaining the parameters were so complicated. In this study, 10 parameters (6 exterior parameters: $dis, \alpha, \beta, \kappa, m_x, m_y$, 4 interior parameters: c_x, c_y, k_1, k_2) were defined to improve the camera calibration. Fig. 2 and Fig. 3 show those parameters and the relations between the object points of the absolute coordinate (X, Y, Z) and the photographical coordinate (x, y, z) of that object. dis means the distance between the origin O(0, 0, 0) and the principle point (X₀, Y₀, Z₀) of the camera on the absolute coordinate. (α, β, κ) is the tilting angle of the axis of the camera coordinate (photographical coordinate) against the axis of the absolute. The coordinate (X_m, Y_m, Z_m) represents the position of the point P when the camera coordinate was rotated with the tilting angles to make the collinear in one line as shown in Fig. 2. The m_x, m_y mean the point at which the normal vector from the origin O(0, 0, 0) of the camera coordinate and the X-Y plane of the absolute coordinate meet. The observational equation that satisfies a collinear condition for every point between the two coordinates could be expressed as Eq. (1).

$$x = c_x \frac{Y_m - m_x}{\sqrt{dis^2 - m_x^2 - m_y^2} - Z_m} + \Delta x \qquad y = c_y \frac{Y_m - m_y}{\sqrt{dis^2 - m_x^2 - m_y^2} - Z_m} + \Delta y \tag{1}$$

Here, c_x and c_y are the focal distances for each component of the coordinate. Δx and Δy are the components of lens distortions as shown in Eq. (2).

$$\Delta x = \frac{x}{r}(k_1 r^2 + k_2 r^4), \quad \Delta y = \frac{y}{r}(k_1 r^2 + k_2 r^4), \quad r = \sqrt{x^2 + y^2} \tag{2}$$

Using an improved Gauss-Newton method (Doh, 1995), all necessary camera parameters were obtained on the bases of the above two equations. The three-dimensional position of a particle could be obtained as an intersection of corresponding perspective rays from the two cameras as shown in Fig. 4. The collinear equation for each camera was given as Eq. 3.
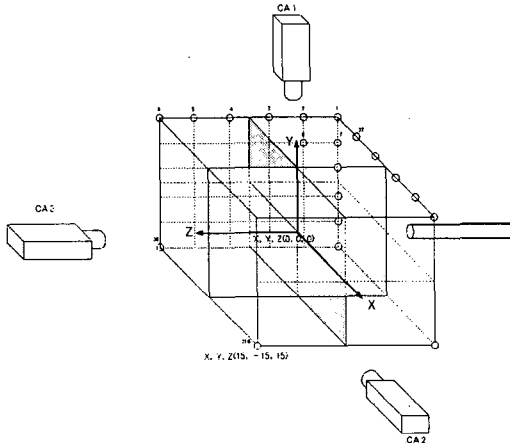

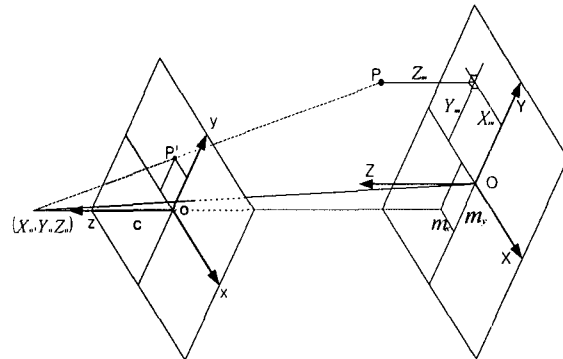**Fig. 1** Calibration landmarks

Fig. 2 Camera parameters and their relations between the absolute coordinate and the photographical coordinate
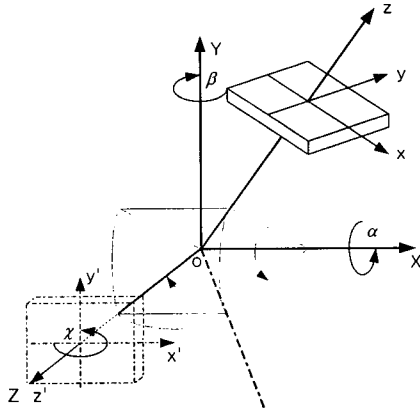
Fig. 3 Relations between the absolute and
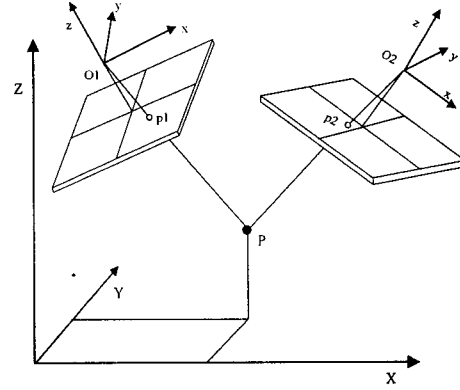the photographic coordinate

Fig. 4 Definition of 3D positions of particles

$$
\begin{pmatrix} X \\ Y \\ Z \end{pmatrix} = \begin{pmatrix} a_{11} & a_{12} & a_{13} \\ a_{21} & a_{22} & a_{23} \\ a_{31} & a_{32} & a_{33} \end{pmatrix} \begin{pmatrix} x \\ y \\ -c \end{pmatrix} + \begin{pmatrix} X - X_o \\ Y - Y_o \\ Z - Z_o \end{pmatrix}
$$

(3)

Here, X, Y and Z are the absolute coordinates transformed from the image coordinates, x and y. c is composed of c_x and c_y. The elements of the rotation matrix a_{ij} were obtained from the camera calibration. Three cameras (A, B, C) were used to get three-dimensional vectors in this study and each two-camera set, (A, B) and (A, C), was contributed to produce the last three-dimensional velocity vectors. Mathematically speaking, since the corresponding perspective rays of the two cameras do not intersect due to unavoidable uncertainties associated not only with the cameras' parameters but also with the particles' centroids, a calculation process in which decision of the coordinate (X, Y, Z) in Eq. (3) was adopted using the least square method. The three-dimensional positions of every particle using the two cameras (A, B) were defined as the following Eq. (4).

$$
\begin{bmatrix} X_P \\ Y_P \\ Z_P \end{bmatrix} = \frac{1}{2} \left\{ \begin{bmatrix} X_A \\ Y_A \\ Z_A \end{bmatrix} + \begin{bmatrix} X_B \\ Y_B \\ Z_B \end{bmatrix} \right\}
$$

(4)

Here, X_A, Y_A and Z_A were defined as the coordinate components that were decided by the use of Eq. (3) for camera A. X_B, Y_B and Z_B were also defined for camera B. In order to calculate the three-dimensional positions of particles, corresponding pairs the centroids of particles of the two camera images should be discovered among many other particles. Below is the genetic algorithm in order to find the corresponding pairs.

2.2 3D-PTV using a Genetic Algorithm

In the conventional 3D-PTVs, the possibility of mismatching particles' pair between the two camera images was so high due to the algorithm themselves. In most of the algorithms adopted, the three-dimensional positions were calculated for all candidates of pairs. In this case, the possibility of dying out of the true pair during the calculation process was relatively high. Here, genetic algorithm has been adopted in order to make the true pairs remain until the whole possible pairs are determined simultaneously.

Table 1 shows the definition of chromosome used in PTV for particles' pairing. Detailed calculation procedure is well explained in the reference (Doh et al., 2001). Four major GA operators, isolation, reproduction, crossover and migration were introduced. A chromosome

9

consists of two coordinates of both cameras. The initial population was generated through a calculation process in which a threshold value was introduced to discriminate the worst particle pairs that had large *3DE* values expressed in Eq. (5).

$$D = \sqrt{(X_B - X_A)^2 + (Y_B - Y_A)^2 + (Z_B - Z_A)^2}$$ (5)

where, $3DE = 1/2(D_s + D_e)$
Ds: 3-dimensional vector error for start point
De: 3-dimensional vector error for end point

Eq. (5) implies that the distance between the two collinears viewed by the two cameras has the minimum value. After the initial population was decided, an isolation process was operated using the same *3DE* value. The particle pairs having a value larger than a threshold *3DE* value were isolated to the unselected group. Next, a reproduction process was made. In the reproduction process, a fitness function based on a continuity concept (Doh et al., 2001) was used for a refinement of the selected group. Finishing the reproduction process, a crossover process was adopted. In this process, the photographical data of the two-dimensional vectors of each camera were exchanged and an elimination process was made referencing the *3DE* value again. In order to give a revival chance to the particles sorted into the inferior group up to now, a migration process was adopted. This process is similar to the initialization process.

Table 1: Definition of chromosome with respect to two sets of cameras

Camera 1		Camera 2		Fitness	
Start point	End point	Start point	End point	3D distance error	Continuity

The above processes are repeated up to 10-15 generations. The threshold value *3DE* is 0.5mm and the crossover portion is 15% among the whole chromosomes generated. During the calculation of GA, operators such as, isolation, reproduction, crossover and migration (this concept belongs to mutation) were recursively used until the last optimized solution of the two objective fitness functions with Eq. (5) and the one based on a continuity concept were found, whch implies the pairs of particles were decided. The three-dimensional velocity vectors were then obtained by dividing the distances between the last paired particles by the time interval Δt.

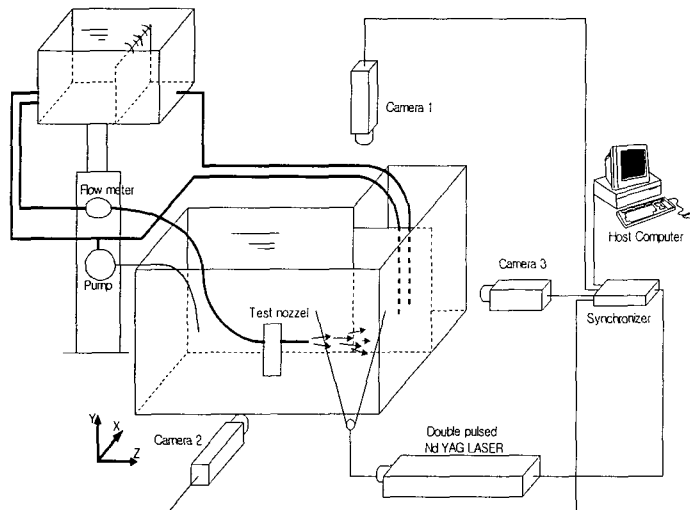## 3. Measurements of the impinging jet

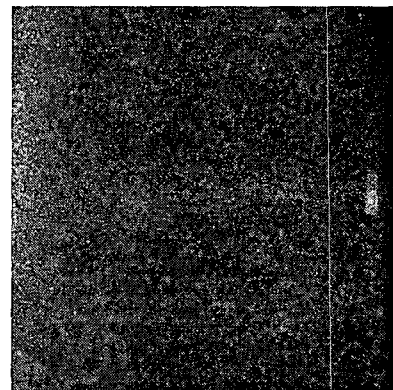Fig. 5 High-Vision 3D-PTV system for the impinging jet

Fig. 6 Raw image viewed by camera 2

10

Fig. 5 shows the overall arrangement for the measurement of the impinging jet. The diameter (d) of the nozzle is 3mm. The measurement system consists of three cameras (Kodak ES1.0, 1,000 x 1,016 pixels), an image grabber (TSI) in the host computer(Pentium III) and a Nd-YAG laser. The three cameras were synchronized with a synchronizer (TSI). The jet was installed in a water tank (800 x 600 x 400mm). A plate (100 x 100mm) was installed in front of the nozzle with a distance of 10d. Reynolds number (UD/v) was about 3,000. v is the kinematic viscosity at 20 ℃. The origin of the absolute coordinate (X=0, Y=0, Z=0) was defined at the center position between the nozzle and the plate along the center line of the jet. The measurement volume is (X:30mm, Y:30mm, Z:30mm). A traverse was used as mentioned for camera calibration and was moved in the volume with 6mm step. After completing the calibration for the three cameras and the construction of the flow field, tracers (Glass Hollow-AG) were seeded into the circulating water channel and a Nd-YAG laser (200mJ) located at a position where the light was backscattering for the three cameras was illuminated. The illuminating time of the laser light is synchronized with the whole camera system. Fig. 6 shows one of grabbed images of the flow pictured by camera 2. Each particle occupies 2-9 pixels on average. Since the pixels of one particle was not so enough to calculate the centroids of the particles, a masking method (Takehara and Etoh, 1999) was used. Fig. 7 shows instantaneous raw velocity vectors obtained by the constructed system. The number of instantaenous 3D vectors obtained was about 6000 with spurious vectors. Spurious vectors were eliminated before the interpolation using Tomson's value (Nishino et al., 1989). The number of vectors regarded as correct ones was about 4000 to 5200. The velocity vectors obtained within the measurement region. The raw vectors were interpolated onto the grids of 16 x 16 x 16 using a Gaussian window (Agui; Jimenez 1987). Fig. 8 shows the interpolated instantaneous three-dimensional vectors on the grids. Fig. 9 shows a time-mean 3D velocity field. And Fig. 10 shows the velocity profiles. The black lines mean the results obtained through a LDV measurement.
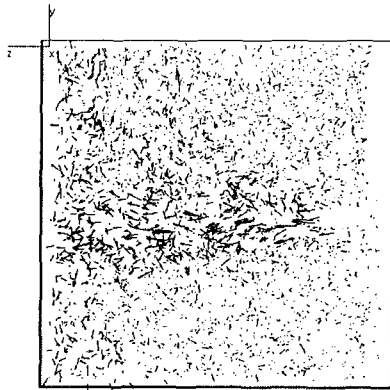

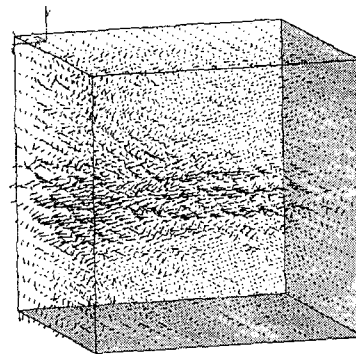**Fig. 7** Obtained instantaneous 3D velocity vectors

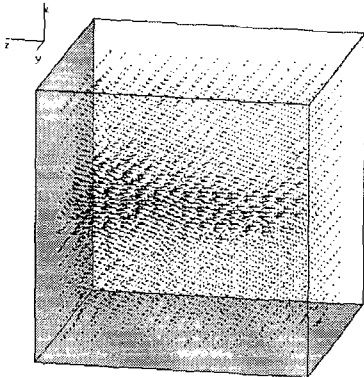**Fig. 8** Instantaneous 3D vectors on grids

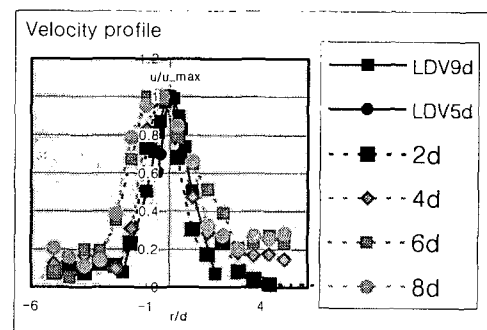**Fig. 9** Time-mean 3D velocity field on grids(16 x 16 x 16)

Fig. 10 Velocity profiles (LDV, 3D-PTV)

11

Fig. 11 Instantaneous vorticity distribution(1-component)
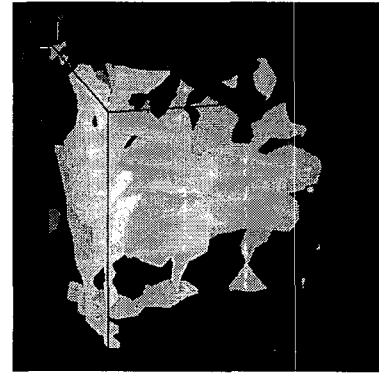(Red = positive, Blue= negative)

Fig. 12 Instantaneous vorticity distribution

The dotted lines with several shape such as square and circle show the results obtained by the constructed 3D-PTV. There are some discrepancies between the results of LDV and those obtained by the 3D-PTV. However, the tendancy is very similar between them. It is estimated that the discrepancies were due to the discrepancy of the nozzle directions when the two experiments, LDV and 3D-PTV were carried out. Fig. 11 shows an instantaneous vorticity distribution of I-component. The results show only one value of vorticity contour. Red colored means positive and and blue one means negative. From this figure, it can be said that there exists minus and plus signed vorticities at an instance among many vorticity values. This quantity will not be able to be captured without a 3D-PTV system. Fig. 12 shows an instantaneous vorticity distribution for the whole components. The vorticity contour dispersed at downstream of the jet. And the vorticity abruptly dispersed near the impinging plate. The constructed High-Vision 3D-PTV system can measure instantaneous vortical structures of any other complex flow.

4. Conclusions

A new High-Vision 3D-PTV technique has successfully been adopted to the measurement of an impinging jet using a genetic algorithm (GA). Using non-metric high-vision three digital cameras, a GA based 3D-PTV was newly constructed for the measurement of complex flows. The vector recovery ratio was fairly good enough to probe the structures of complex flows. In the measurement, about more than 5000 instantaneous three-dimensional velocity vectors could be obtained from about 10000 particles in the measurement region. This implies that the recovery ratio is quite high. If the OS system of the host computer is improved, the recovery ratio will be even more higher. This percentage is the most highest among other three-dimensional PTV techniques up to now, which also implies the possibility of direct probing of flows if more high-definition cameras and video systems are adopted. The properties of the impinging jet obtained by the constructed High-Vision 3D-PTV system showed qualititatively reasonable. The velocity profiles obtained by the GA-3D-PTV system showed qualitative agreements with those of LSV measurements. The constructed system will be able to be used for the investigation of the turbulent properties of complex flows such as wakes, jets and other complex flows.

Acknowledgements

References
Adrian R J (1991) Particle-imaging techniques for experimental fluid mechanics, Ann. Rev. Fluid Mech. Vol.23, pp.261-304.
Agui J C; Jimenez J (1987) On the performance of particle tracking, J. Fluid Mech., Vol. 185, pp.447-468.
Ballard D H; Brown C M (1982) Computer Vision, Prentice-Hall, New Jersey, pp.195-225.

Burmeister L C (1983) Convective Heat Transfer, Wiley, New York.

Doh D H (1995) A study on three dimensional particle imaging thermometry and velocimetry using liquid crystal, PhD Thesis., Tokyo Univ.

Doh D H; Kim D H; Choi S H; Hong S D; Saga T; Kobayashi T (2000) Single-Frame (Two-Field Image) 3D-PTV for high speed flows, Exp. in Fluid, Suppl., pp.85-98.

Doh D H; Kim D H;.Cho K R; Cho Y B; Saga T; Kobayashi T (2001) 3D-PTV using Genetic Algorithm, Proc. CD-ROM of 4th International Symposium on PIV, Gottingen, Sep. 17-19, 2001, Paper No.A1050.

Faggiani S; Grassi W (1990a) Impinging Liquid Jets on Heated Surfaces, Proceedings of the Ninth International Heat Transfer Conference, Vol.1, pp.275-285.

Faggiani S; Grassi W (1990b) Round Liquid Jet Impingement Heat Transfer: Local Nusselt Numbers in the Region With Non Zero Pressure Gradient, Proceedings of the Ninth International Heat Transfer Conference, Vol. 4, pp. 197-202.

Goldberg D E (1985) Optimal initial population size for binary-coded genetic algorithm, TCGA Report No. 85001. University of Alabama.

Gardon R; Akfrat J C (1965) The role of turbulence in determining the transfer characteristics of impinging jet. Int. J. Heat Mass Transfer, Vol. 8 pp.1261-1272.

Hwang S D; Lee C H; Cho H H (1999) An Experimental study on flow and heat transfer characteristics of circular impinging jet with acoustic excitation, Proceeding of KSME thermal engineering. pp.122-129.

Kasagi N; Nishino K (1991) Probing turbulence with three dimensional particle tracking velocimetry, Exp. Thermal and Fluid Sci. Vol.4, pp.601-612.

Kataoka K; Mihata I; Maruo K; Suguro M; Chigusa T (1986) Quasi periodic large scale structure responsible for the selective enhancement of impinging jet heat transfer, Proceeding of the 8th Int. Heat Transfer Conf. Vol. 3, pp.1193-1198.

Kiper A M (1984) Impinging Water Jet Cooling of VLSI Circuits, International Communications in Heat and Mass Transfer, Vol.11, pp.517-526.

Lee J H; Lee S J (1999) Heat transfer enhancement based on nozzle exit configuration of turbulent axisymmetric impinging jet, Proceeding of KSME thermal engineering. pp.122-129.

Mass H G; Gruen A; Papantoniou D A (1993) Particle tracking velocimetry in three-dimensional flows, Part 1 Photogrammetric determination of particle coordinates. Exp. in Fluids, Vol.15, pp.133-146.

Nishino K; Kasagi N; Hirata M (1989) Three-dimensional particle tracking velocimetry based on automated digital image processing, ASME J. Fluids Eng., Vol.111 No.4, pp.384-391.

Nakoryakov V E; Pokusaev B G; Troyan E N (1978) Impingement of an Axisymmetic Liquid Jet on a Barrier, International Journal of Heat and Mass Transfer, Vol.21,pp.1175-1184.

Olsson, R G; Turkdogan E T (1966) Radial Spread of a-Liquid Stream on a Horizontal Plate, Nature, Vol.211, pp.813-816.

Ohyama R; Takagi T; Tsukiji T; Nakanishi S; Kaneko K (1993) Particle tracking technique and velocity measurement of visualized flow fields by means of genetic algorithms, Journal of Flow Visualization Soc. Jpn., Vol.13 Suppl. No.1, pp.22-25.

Sibulkin M (1952) Heat Transfer Near the Forward Stagnation Point of a Body Revolution," Journal of the Aeronautical Sciences, Vol.9, pp. 570-571.

Stevens. J; Webb B W (1991) Local Heat Transfer Coefficients Under an Axisymmetric, Single-Phase Liquid Jet. ASME, Heat Transfer, Vol. 113, pp. 71-78.

Stevens J (1992) Measurements of Local Fluid Velocities in an Axisymmetric. Free Liquid Jet Impinging on a Flat Plate. Ph.D. Dissertation. Brigham Young University, Provo. UT.

Takehara K; Etoh T (1999) A study on particle identification in PTV –Particle Mask Correlation Method-, Journal of Visualization, Vol.1 No.3, pp.313-323.

Vader D T; Incropera F P; Visskanta R (1991) Local Convective Heat Transfer From Heat Surface to an Impinging Planar Jet of Water, International Journal of Heat and Mass Transfer. Vol. 34, No. 3. pp.611-623.

Yamada H; Yamane K (1995) Particle Image Velocimetry Using a Genetic Algorithm, J. of Flow Visualization Soc. Jpn., Vol.15, Suppl. No.1, pp.165-168.

Yamamoto H; Udagawa Y; Suzuki M; (1987) Cooling System for FACOM M-780 Large-Scale Computer," Procreedings of the International Symposium on Cooling Technology for Electronic Equipment , pp.96-109.